International Journal of Impact Engineering 76 (2015) 75–82

Contents lists available at ScienceDirect

International Journal of Impact Engineering

journal homepage: www.elsevier.com/locate/ijimpeng

Effect of inter-layer toughness in ballistic protection systems on absorption of projectile energy

E.K. Öberg, J. Dean, T.W. Clyne*

Department of Materials Science & Metallurgy, Cambridge University, 27 Charles Babbage Road, Cambridge CB3 0FS, UK

ARTICLE INFO

Article history:
Received 14 May 2014
Received in revised form
28 July 2014
Accepted 16 September 2014
Available online 28 September 2014

Keywords:
Impact
Interfacial toughness
Energy absorption
Layered systems

ABSTRACT

This paper concerns absorption of the kinetic energy of a projectile in multi-layer protection systems, with particular focus on the role of inter-layer bonding. Two-layer samples have been produced, composed of a 2 mm thick alumina front plate and a carbon fibre composite back plate with a thickness of about 0.8 mm. These were manufactured under two sets of conditions. The fracture energy of the inter-layer interface was measured for these two types of sample to be 170 and 620 J m^{-2}. Such samples were subjected to impact by spherical projectiles of hardened steel, with a diameter of 8 mm and an impact speed of about 220 m s^{-1}, corresponding to a kinetic energy of about 50 J. Samples composed of the alumina plate alone and of unbonded alumina and composite layers were also tested. It was found that significantly more projectile energy was absorbed by the strongly bonded samples, and that this difference was greater than could be explained solely in terms of the interfacial debonding energy. This is investigated by estimating the magnitudes of all of the identifiable sources of energy absorption, including that of plastic deformation of the projectile. It is concluded that strong inter-layer bonding can promote greater energy absorption in the composite back-plate.

1. Introduction

There has been extensive work [1–8] on the development of systems offering protection against damage from projectile impact. Most of these are based on multi-layer structures, with a front plate made of a hard material (designed to resist the initial impact of the projectile) and a layer, or layers, behind this, in which the energy of the projectile becomes dissipated. In combination, such systems are designed to impede penetration of the projectile and also to ensure that there is minimal transmission of energy and momentum to the region being protected. Low weight is often desirable and it's become common to use ceramic (often alumina) front plates and tough, polymer-based composite layers in the energy-absorbing role.

Sometimes a layer (usually quite thin and often termed a ***confinement layer***) is incorporated immediately behind the front plate, with a primary function of ensuring that, after impact, the front plate remains in place, even if it becomes fragmented. It is often made of a relatively tough material that is likely to remain intact after impact and there is usually a strong bond with the front plate. The main role of the confinement layer is to confer a good "second strike" resistance [9] on the structure – ie to ensure that the front plate remains sufficiently integral to prevent easy passage of a second projectile that might arrive close to the site of the initial impact.

Attempts are usually made to ensure that the confinement layer is well bonded to the front plate, since this is logical in terms of its primary function. In general, however, it's not very clear whether the overall performance of the system is enhanced by making all interfacial bonding as strong (or tough) as possible. In fact, there is probably an argument to be made along the lines that weak bonding, and hence extensive delamination on impact, could assist in spreading the energy dissipation over a greater area. In practice, while there have been a number of studies [10–15] focussed on energy absorption during ballistic impact of layered structures, there has been only rather limited (experimental or theoretical) examination of this issue [16,17], mainly because there is inevitably a complex interplay between the various phenomena that occur during ballistic impact of a multi-layer protection system, with a substantial number of experimental variables and potential complications. Also, it is relatively uncommon to control and quantify the inter-layer strength (toughness) in a systematic way. The present paper is aimed in this direction, focussing on a simple two-layer system with two (significantly) different levels of inter-layer

* Corresponding author. Tel.: +44 1223 334332.
E-mail address: twc10@cam.ac.uk (T.W. Clyne).

http://dx.doi.org/10.1016/j.ijimpeng.2014.09.006
0734-743X/

bond strength and making an attempt to measure and understand the various contributions to the absorbed energy for the two different cases.

2. Experimental procedures

2.1. Material

The alumina plates, supplied by Hybrid Laser, were 2 mm thick and had a density of 3.84 g cm^{-3} – measured using helium-pycnometry (Micrometrics Accupyc 1330). X-ray diffraction revealed that they were composed mainly (~96%) of α-alumina, with the remainder being a spinel. The surface roughness was measured (using a Dektak 32 stylus profilometer) to have an R_a value of ~1 μm. A fracture surface is shown in Fig.1, where it can be seen that fracture is inter-granular and the grain size varies between about 3 and 10 μm.

A commercial woven fibre composite (Comfil®) was employed as a backing (confinement) layer. It has a 2 × 2 twill weave structure with 0.33 tows mm^{-1}, as shown in Fig. 2. The tows consist of 12 K *Tenax* HTS carbon fibres (6–8 μm diameter) and (low density) polyethylene terephthalate (PET) fibres (~30 μm diameter), intertwined in each of the yarns. The PET fibres soften when heated. At sufficiently high temperatures, and under the action of applied pressure, the PET flows and infiltrates the open spaces, forming a thermoplastic matrix. The consolidated thickness of a single composite ply was ~0.78 mm, with a density of 1.54 g cm^{-3}.

2.2. Production of layered specimens by hot pressing

Layered specimens were manufactured by hot pressing, using an applied pressure of 30 bar. Two hot pressing temperatures were employed – 200 °C and 230 °C. Prior to hot pressing, the alumina was cleaned with detergent and ethanol, before being submerged in an ultrasonic bath for 20 min.

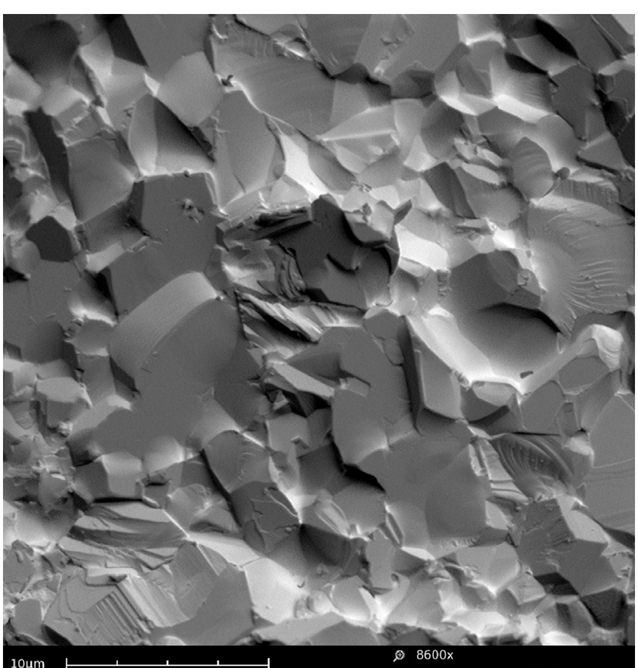

Fig. 1. SEM micrograph of a fracture surface from an alumina plate.

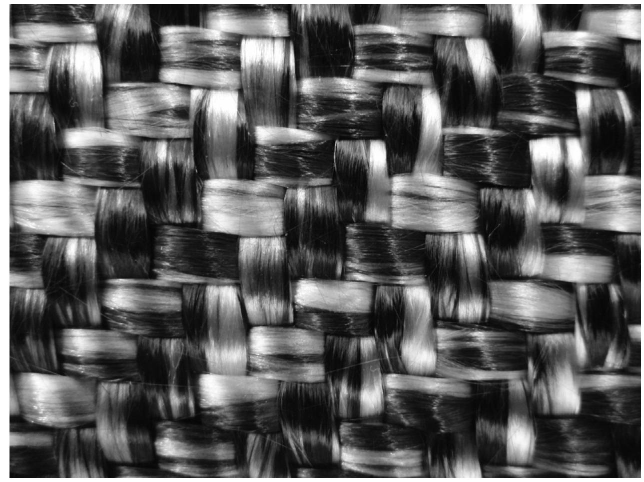

Fig. 2. Optical micrograph of the free surface of C-PET twill woven ply, before consolidation.

2.3. Alumina fracture energy measurement

The fracture energy of the alumina plates was measured using the Charpy impact test. The specimen sizes were 15 × 5 × 50 mm. The samples were pre-notched, with a notch depth of 1.5 mm. To calibrate the apparatus, the pendulum was allowed to swing without the sample present, and the energy loss due to friction alone was measured at 0.01 J. Compared to typical measured values of the fracture energy, this was found to be negligible and could be ignored. Cases in which fracture did not take place from the notch were excluded.

2.4. Inter-layer fracture energy measurement by 4-point bend delamination

To measure the inter-layer fracture energy (between the alumina and the C-PET layer) the 4-point bend delamination test, as developed by Charalmbides et al. [18] and Howard and Clyne [19], was employed. This test tends to produce strongly "mixed mode" fracture conditions. The stiffness of the C-PET layer was enhanced by the addition of a Ti–6Al–4V layer, with a thickness of 1 mm. (Without this, the energy released by inter-layer debonding would have been insufficient to drive an inter-layer crack, particularly with a relatively tough interface: the effect of the stiffening element is incorporated in the analysis.) The titanium alloy sheets were sand-blasted, in order to create rough surfaces that allowed the bond between the titanium and the C-PET to be tough enough to ensure that delamination occurred (only) between the alumina layer and the C-PET layer. The measured R_a value for the sand-blasted titanium alloy was ~3.6 μm, which is ~3.5 times greater than that obtained for the alumina. The yield stress of the titanium alloy sheet (~1 GPa) is high enough to ensure that it did not undergo any plastic deformation during the testing.

Any excess polymer, visible around the edges of the specimens after hot pressing, was removed prior to testing, in order to prevent residual polymer ligaments from forming across the de-bonding interfaces. A pre-crack along the interface between the alumina and the C-PET ply was introduced by adding thin kapton sheets (7 mm in length on either side of the notch in the alumina) before hot pressing. In all cases, it was found that the inter-layer crack did indeed propagate between the alumina and C-PET layers, and the Ti alloy sheets remained bonded to the C-PET layers throughout.

The specimens were tested using a motor-controlled set-up, under displacement control. Displacements were measured using a scanning laser extensometer with a resolution of ~1 μm. Specimen lengths were typically about 160 mm. The distance between the outer rollers was fixed at ~140 mm, while that between the inner rollers was ~70 mm. Load and displacement histories were continuously monitored. A specimen, after testing, is shown in Fig. 3(a). Visible in this micrograph are: i) the three layers (including the Ti alloy sheet added to stiffen the C-PET layer), ii) the notch in the alumina and iii) a de-bonded region between the alumina and the C-PET. A close-up of an inter-layer region that remained bonded during testing is shown in Fig. 3(b). It can be seen that the polymer became sufficiently soft during hot pressing to penetrate the depressions in the rough alumina surface, creating a well-bonded interface.

2.5. Ballistic impact testing

Ballistic impact tests were conducted using a gas gun. The projectile was made of a 52100 type steel, containing ~1.3–1.6 wt% Cr, 0.95–1.1 wt%C and small amounts of Mn and Si. The microstructure is martensitic, with cementite spheres, typical of quenched and tempered chrome steel for ball bearings. The high C content ensures that this steel has a relatively high hardness. Spherical projectiles were used, with 8 mm diameter, mass of ~2 g and an impact velocity of about 220–230 m s^{-1}, giving an incident projectile kinetic energy of about 50 J. Incident and emergent projectile velocities were measured (with a precision of about ±1%) using two pairs of light gates. Specimens were clamped inside a steel frame, confined along their edges, leaving a free (exposed) surface measuring 64 × 64 mm. Specimen in-plane dimensions were 70 × 70 mm. The alumina plates were 2 mm thick in all cases, while all of the C-PET layers were about 0.8 mm in thickness.

Four different types of specimen were employed. These were:

(i) Alumina plate alone
(ii) Alumina plate and (consolidated) C-PET layer, clamped together around the frame, but not bonded together
(iii) Bonded alumina plate plus C-PET layer, produced by hot pressing at 200 °C
(iv) Bonded alumina plate plus C-PET layer, produced by hot pressing at 230 °C

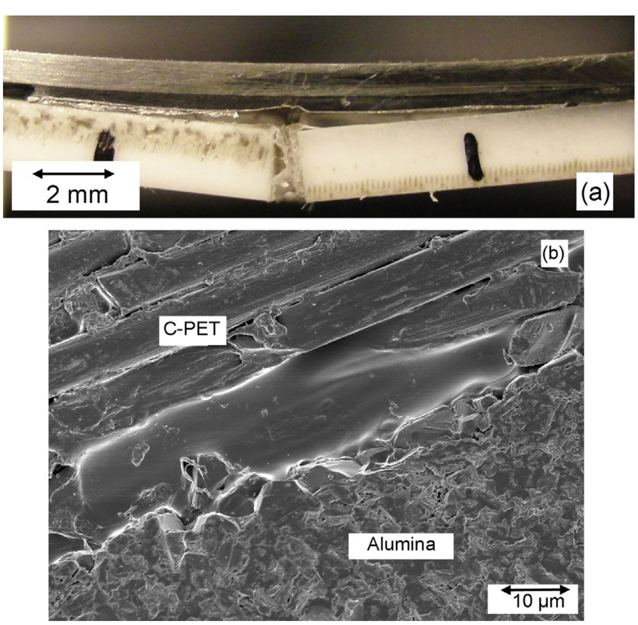

Fig. 3. Micrographs from a 4-point bend delamination specimen (with high bond strength), taken from the side after testing: (a) an optical micrograph showing most of the specimen and (b) an SEM micrograph of the interfacial region between the alumina plate and the bonded C-PET layer, beyond the interfacial crack.

3. Alumina and inter-layer fracture energies

3.1. Alumina fracture energy

Measured fracture energy values, obtained by Charpy testing, are shown in Fig. 4. It can be seen that typical values were ~2–3 kJ m^{-2}. This is a little higher than might have been expected for alumina under ideal plane strain, mode I conditions, but they are similar to values obtained previously [20] for alumina by Charpy testing. Of course, fracture propagation during ballistic testing probably does not occur under plane strain, mode I conditions either, and the cracking stimulated during the Charpy test does at least occur as a result of an impact event.

3.2. Inter-layer fracture energy

Typical load–displacement curves obtained during 4-point bend testing are shown in Fig. 5(a). Two types of specimen were tested, having been produced by hot pressing at either 200 °C or 230 °C. It's clear that, in all cases, there is a distinct plateau in the plot, corresponding to regimes of at least approximately steady state crack propagation. These are expected to yield valid fracture energy values. There is also evidence for short periods of "crack-bursting", indicating that there were some variations in the local toughness of the inter-layer interface. Derived values of the inter-layer fracture energy are shown in Fig. 5(b). For the specimens processed at 200 °C, an average G_{ic} value of ~170 J m^{-2} was obtained, whereas the corresponding figure for samples pressed at 230 °C is ~620 J m^{-2}. It's thus clear that inter-layer interfaces created under the latter conditions were appreciably tougher. Of course, interfacial debonding during projectile impact may absorb rather different amounts of energy, due to the higher speed of crack

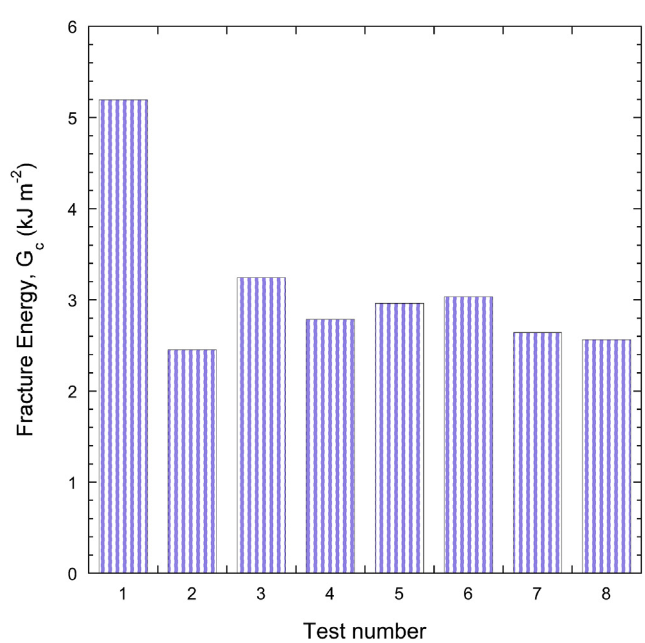

Fig. 4. Fracture energy of alumina, as measured with the Charpy impact test.

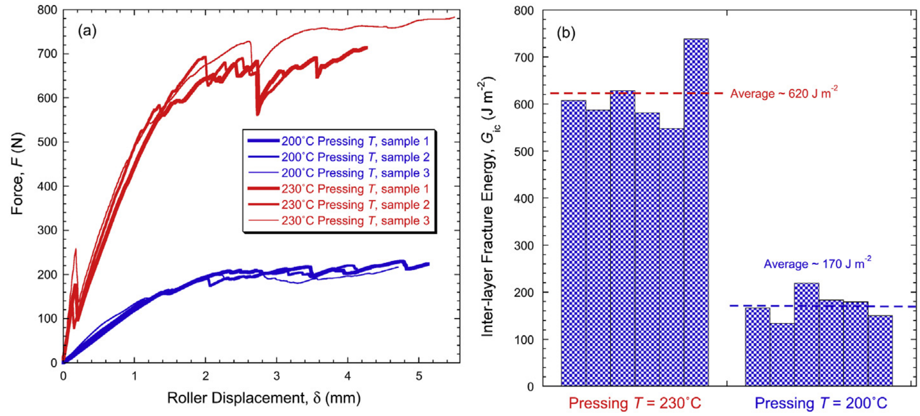

Fig. 5. Data from 4-point bend delamination testing, in the form of (a) typical load–displacement plots and (b) deduced inter-layer fracture energy values, for specimens produced using two different hot pressing temperatures.

propagation, but the change is unlikely to be massive and it's still expected that the interface created at the higher processing temperature will be tougher.

4. Work of plastic deformation of the projectile

The energy absorbed within a metallic projectile (such as this steel) is likely to be dominated by plastic deformation, and thus determined largely by its yielding and flow characteristics. These parameters are usually quite sensitive to strain rate. This sensitivity is difficult to measure using conventional mechanical testing procedures and the difficulties are compounded by the complex nature of the evolving strain and strain rate fields in spherical test specimens.

Nevertheless, it is possible to estimate the plastic work done within a projectile, taking account of its strain rate sensitivity, from its deformed shape, by using numerical modelling and assuming a functional form for the strain rate dependence of the plastic deformation. This is a reasonably tractable problem, particularly if there is radial symmetry, such as for a spherical projectile at normal incidence to a flat surface (as in the present case). Projectiles of 52100 steel were fired at an alumina rod, striking it normal to one of its flat ends with an impact velocity of 110 m s^{-1}. The alumina rod was 150 mm in length and 46 mm in diameter, and thus large in comparison with the projectile. This ensured that the absorbed energy was predominantly dissipated through plastic deformation of the projectile, and not through other mechanisms (such as fracture of the alumina). Indeed, after impact, there was little noticeable damage to the alumina at the point of impact. (This was not the case when significantly higher impact velocities were used.)

The deformed projectile shapes were characterised by tracking a Dektak profilometer over the flattened surface and for a short distance around the adjoining (approximately) spherical surface. The deformed shape was radially symmetric (with the axis of symmetry being the original flight direction), at least to a good approximation. The profilometer tracks passed through this axis of symmetry. Measurements were also made, using callipers, of the distance between the centre of the flattened surface and the diametrically opposite surface of the sphere – ie along the axis of radial symmetry. This provided a datum for the centre of the Dektak profile.

A finite element model was created, comprising the alumina rod and the spherical projectile. The ceramic was modelled as an elastic body (free to undergo elastic compression and extension, without damping) and there was no attempt to model any damage to the alumina occurring during impact. The Young's modulus of the ceramic was set to 340 GPa. The projectile, on the other hand, was modelled as a plastically-deformable body of linear elements, with plasticity being defined using the strain rate-dependent (empirical) formulation of Johnson & Cook [21,22]. It was assumed that 95% of the plastic work done within a volume element during the time increment concerned was released within the element as heat, the redistribution of which was modelled using a thermal conductivity for steel of 46.6 W m^{-1} K^{-1}. It was also assumed that, while thermal conduction occurred within the projectile, there was no heat transfer to the surroundings (air or alumina rod). No fracture criterion was specified for either the projectile or the rod and friction between them was ignored. The values of the parameters employed in the Johnson–Cook formulation for this steel are presented in Table 1 (obtained from a range of sources).

5. Effect of inter-layer toughness on energy absorbed in ballistic impact

5.1. Experimental outcomes

Experimental data are presented in Fig. 6(a) for the loss of projectile kinetic energy as penetration took place through a number of samples of the four different types (Section 2.5). It can be seen that the approximate average energy losses for the 4 types of sample were as follows: (i) alumina plate alone: ~15 J, (ii) unbonded alumina + C-PET: ~29 J, (iii) alumina + C-PET bonded at 200 °C: ~30 J and (iv) alumina + C-PET bonded at 230 °C: ~40 J. In general, these values appear to be fairly reproducible. Their magnitudes are considered in the next section.

Table 1
Values of the Johnson–Cook formulation parameters used for the 52100 steel.

Parameter	Value
Density, ρ	7800 kg m^{-3}
Young's modulus, E	200 GPa
Poisson's ratio, ν	0.3
Static yield stress, A	1400 MPa
Work hardening rate, B	1500 MPa
Work hardening exponent, n	0.19
Temperature dependence exponent, m	0.66
Strain rate sensitivity parameter, C	0.027
Transition temperature, T_{trans}	293 K
Melting temperature, T_m	1673 K
Reference strain rate, $(d\varepsilon/dt)_0$	0.001 s^{-1}
Specific heat, C_p	475 J kg^{-1} K^{-1}

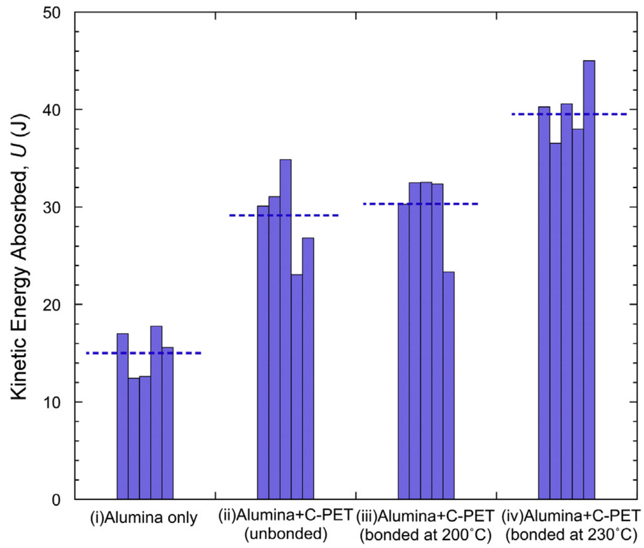

Fig. 6. Histogram showing projectile energy loss values for penetration of steel spheres through specimens of types (i) – (iv).

5.2. Energy-based analysis

5.2.1. Overview

Of course, the impact and penetration of a projectile on and through a multi-layered plate involves various complex phenomena. These are not, in general, readily amenable to (energy-based) analysis, even when, as in the present case, the impact velocity is sub-sonic, all materials are isotropic, the projectile is spherical, the projectile does not break up on impact and the sample is a simple two-layer structure (or a monolithic plate). Nevertheless, by making certain assumptions, a straightforward analysis can be carried out. Central to these is the idea that the absorbed energy can be broken down into several component contributions, which, at least as a working hypothesis, are independent of each other. The energy absorbed (loss of kinetic energy of the projectile) may in the present case thus be expressed as.

$$U_{\mathrm{absorbed}} = U_{\mathrm{projectile}} + U_{\mathrm{alumina}} + U_{\mathrm{C-PET}} + U_{\mathrm{interface}} \tag{1}$$

in which the terms on the right hand side respectively represent the energies absorbed: (a) within the projectile itself (via plastic deformation), (b) in the alumina front plate, (c) in the C-PET backing (confinement) plate and (d) within the interface between these two layers (as debonding occurs). Possibly there would be a contribution from energy absorption in the frame holding the sample in place, but this is expected to be small and more or less independent of the type of sample. These contributions are now considered in turn, with the clear understanding that the energy values should not be regarded as doing much more than giving an order of magnitude for the term concerned.

5.2.2. Work of plastic deformation of the projectile

Predicted contours of residual von Mises stress in the projectile, after striking an alumina rod at 110 m s^{-1}, are shown in Fig.7. Predictions of the deformed projectile shape are compared to the experimental data in Fig. 8. The agreement is quite good, which suggests that the parameters in Table 1 provide a reasonably accurate description of the material behaviour. The energy absorbed by the projectile during impact of an alumina-CPET composite can therefore be estimated by modelling such an event, using the (validated) parameters in Table 1 to describe the rate-sensitive behaviour of the 52100 steel (as described in Section 4).

A second finite element model was then created, incorporating the complete C-PET/alumina system. The (2 mm thick) ceramic was modelled as an elastic body (free to flex), clamped rigidly around its (square) perimeter, with $E = 340$ GPa and $\nu = 0.2$. A criterion for fracture was not included, so the predicted energy absorbed by projectile deformation should be treated as an upper bound. The C-PET layer was modelled by creating a lamina layer in ABAQUS, comprising a single ply (0.8 mm thick) modelled as a shell. The in-plane Young's modulus values [23] were fixed at $E_1 = E_2 = 45$ GPa. The alumina and C-PET layers were rigidly bonded. The projectile was modelled as a plastically deformable body, using the Johnson–Cook formulation and the (validated) parameter values in Table 1. Friction between the ceramic and the projectile was neglected. The predicted von Mises stress field 1 µs after impact are shown in Fig. 9. The relevant outcome is that, for the velocity of interest here (~220 m s^{-1}), the (maximum) energy absorbed via plastic deformation of the projectile was about 6.8 J. Accepting that this is an order of magnitude analysis, a value of ~5 J is used in the energy audit.

5.2.3. Work of fracture of the alumina plate

Given the fracture energy of the alumina (~2–3 kJ m^{-2} – see Fig. 4), this contribution just requires estimation of the area over which cracking occurred within the plate. Unfortunately, this is rather complex, since little is known about what happened inside the volume of alumina punched out by the projectile. There is, however, a (crude) way of estimating this, since, in the case of sample type (i), only the first two terms in Eqn. (1) can contribute. It therefore follows that the difference between the total energy absorbed (~15 J) and the energy of plastic deformation of the projectile (~5 J), ie about 10 J, is attributable to (fracture) processes taking place within the alumina plate during penetration by the projectile. Moreover, as can be seen in Fig. 10, the cracking patterns in the region around the punched hole are rather similar with and

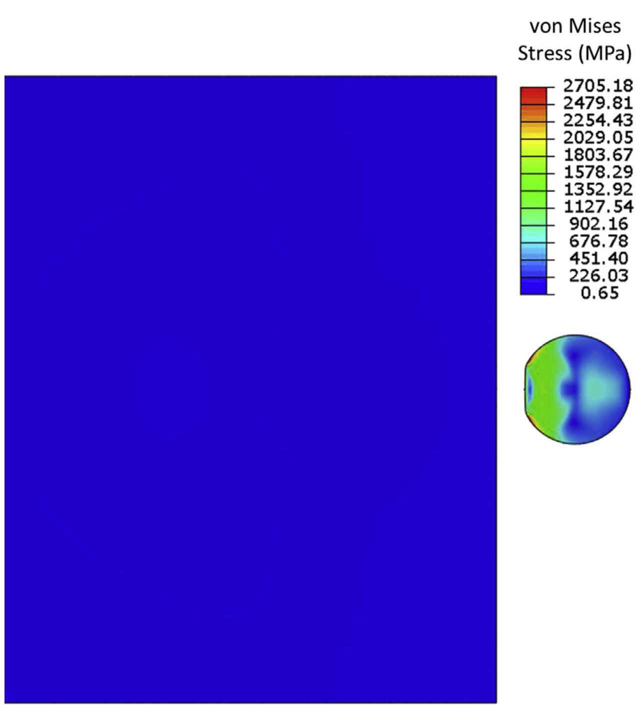

Fig. 7. Predicted residual projectile shape and von Mises stress field after striking a long rod of alumina at 110 m s^{1}.

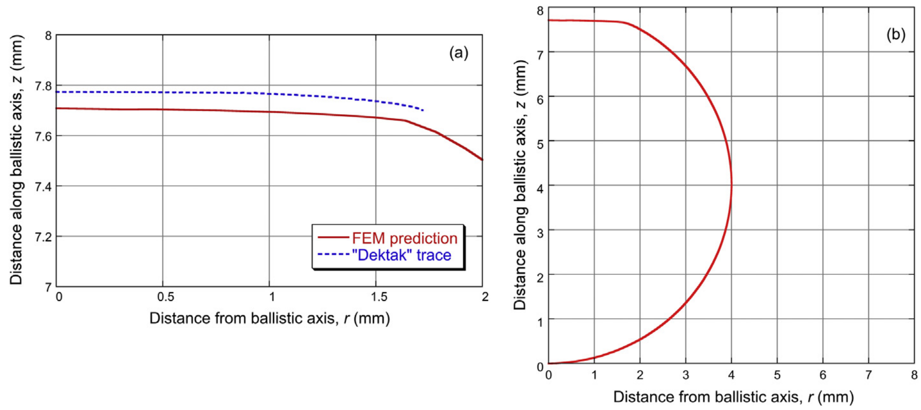

Fig. 8. Predicted and measured projectile profiles after ballistic impact of a 52100 steel at 110 m s^{-1}, showing (a) comparison with experiment for the shape of the plateau region and (b) predicted overall shape.

without a backing (confinement) layer. (For the type (i) sample shown in Fig. 10(a), a thin adhesive layer was attached to the back of the alumina plate, which would have had a negligible effect on the cracking behaviour, but held the fractured fragments in place – as the confinement layer did for the other samples.) Estimates of the aggregate crack length visible in the micrographs shown in Fig. 10 give a value of the order of 500 mm, corresponding (for a plate thickness of 2 mm) to a crack area of ~10^{-3} m^2. Using a G_c value of 2 kJ m^{-2} for the alumina, this gives an energy value of about 2 J. It follows that something like 8 J was absorbed via the fragmentation and pulverisation processes that occurred in the punched-our region (and possibly including a contribution from the kinetic energy of these expelled fragments).

5.2.4. *Work of deformation and fracture of the C-PET layer*

The energy absorbed during deformation and fracture of the composite layer is very difficult to deduce from known or measurable properties. However, it is again possible to infer the contribution from the measured energies for the cases examined. The difference between type (ii) and type (i) situations (ie about 14 J) can be assumed to arise solely from the presence of the composite layer. It has a relatively high toughness (largely associated with fibre pull-out) and, given that there was a substantial amount of deformation and fracture in the punched-out region, and also in the surrounding area, this value seems plausible, despite the fact that the layer was relatively thin.

5.2.5. *Work of inter-layer debonding*

Consideration of the data for the type (iii) and type (iv) samples allows focus on the effect of the bonding between the front plate and the confinement layer. Since the interfacial fracture energy is known, for the two different processing conditions, an upper bound can be placed on the direct contribution from this source, on multiplying the exposed area (64 × 64 mm = 4096 mm^2), minus the punched-out area (~100 mm^2), by the interfacial fracture energy concerned (170 J m^{-2} or 620 J m^{-2}). This gives ~0.7 and 2.5 J respectively for type (iii) and type (iv) cases. It can be seen that these contributions are relatively small, which is at least consistent with the absorbed energy values for types (ii) and (iii) being very similar (~29 and 30 J). However, it's noticeable that there is what appears to be a significant difference (~10 J) between the type (iii) and type (iv) cases. This looks too large to be explicable solely in terms of the (maximum) difference between the direct contributions from debonding, which is less than 2 J. A possible conclusion is that strong inter-layer bonding affects other mechanisms of energy absorption. For example, it might lead to more energy being absorbed during deformation and fracture of the C-PET layer. Observed differences in appearance of the layer after projectile penetration for the two cases, apparent in Fig. 11, might be consistent with this.

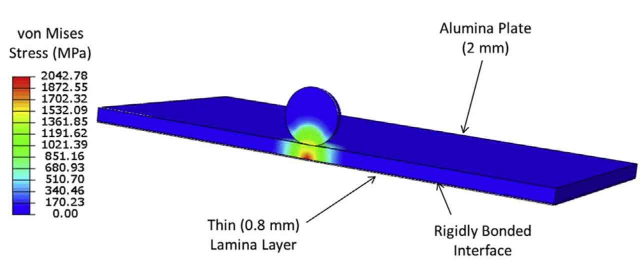

Fig. 9. Predicted von Mises stress field 1 μs after a projectile has struck an alumina/C PET layered system with a velocity of 220 m s^{-1}.

5.2.6. *Summary*

The energy contributions are summarised graphically in Fig. 12. The main objective of the current work, apart from exploring the feasibility of carrying out an energy audit of this type, is to examine the effect of inter-layer bond toughness on the overall performance of a ballistic protection system. Of course, the system under study has been simplified, not only in terms of having a spherical projectile, but also by removing an important component of a practical multi-layer system – ie the energy-absorbing layer at the back. Nevertheless, some interesting observations might be possible. In particular, it would appear that a tough bond between the front plate and the confinement layer can affect the overall behaviour, beyond just absorbing more energy via debonding. This is plausible, since improved bond strength is likely to affect the constraint imposed on other deformation and fracture mechanisms. From the limited information available here, this has led to enhancement of the energy absorbed in deformation and fracture of the composite (confinement) layer, rather than in fracture of the alumina front plate, although this is somewhat speculative. It's unclear whether an enhancement would occur in the performance of a more substantial energy-absorbing back layer, if it were present, although it seems possible.

6. Conclusions

The following conclusions can be drawn from this work.

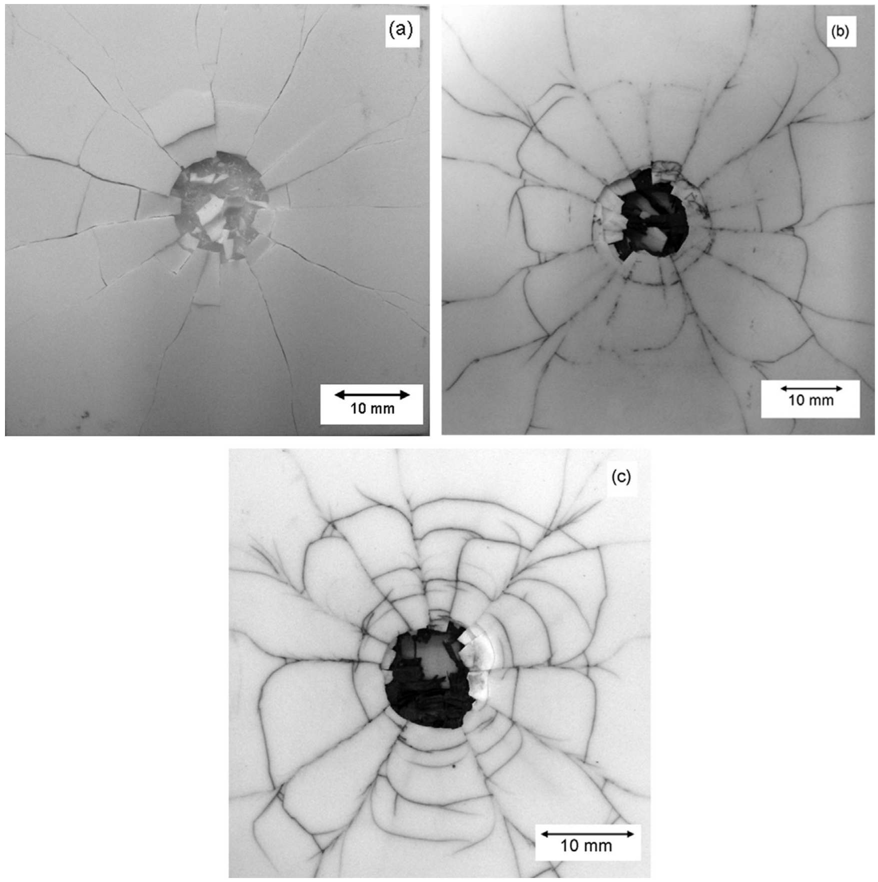

Fig. 10. Optical photographs of the front surfaces of alumina plates, after projectile penetration, from typical specimens of (a) type (i) – ie alumina only – (b) type (iii) – ie alumina weakly bonded to C-PET – and (c) type (iv) – ie alumina strongly bonded to C-PET.

(a) Bi-layer (alumina-carbon fibre composite) samples have been produced, using two hot pressing temperatures, and the corresponding interfacial fracture energy values obtained using the 4-point bend delamination test. These values were found to be around 170 and 620 J m^{-2}.
(b) Samples were impacted with small (8 mm diameter) spherical projectiles of hardened steel. Measured incident and emergent projectile velocities were used to obtain the energy absorbed with these samples, and also with samples of alumina alone and a bi-layer having no interfacial bonding. These energies were about 15 J for the alumina, 30 J for both the unbonded and the weakly bonded samples and 40 J for the strongly bonded samples. Using the measured interfacial fracture energy values, the energy needed to completely debond the weakly and strongly bonded samples can be estimated as 0.7 and 2.5 J respectively.
(c) A procedure involving finite element modelling has been used to estimate the energy absorbed by plastic deformation of the projectile. This turned out to be ~5 J for all of the samples. Together with the measured levels of absorbed energy for the four types of sample, this allowed the energy from cracking in the alumina plate to be estimated at ~10 J and that from deformation and damage of the composite plate (in the absence of strong bonding) to be estimated at ~15 J.
(d) It can thus be inferred that, for the conditions of these tests, strong inter-layer bonding raises the energy absorbed within the sample, by an amount that is greater than can be

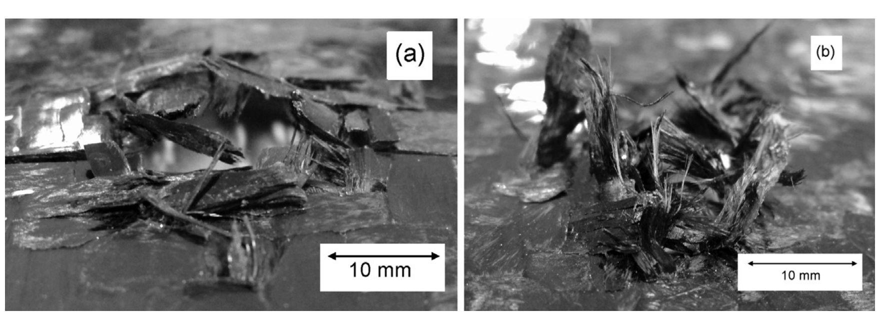

Fig. 11. Optical photographs of the back surface of samples after projectile penetration for (a) a type (iii) sample – bonded at 200 °C – and (b) a type (iv) sample – bonded at 230 °C.

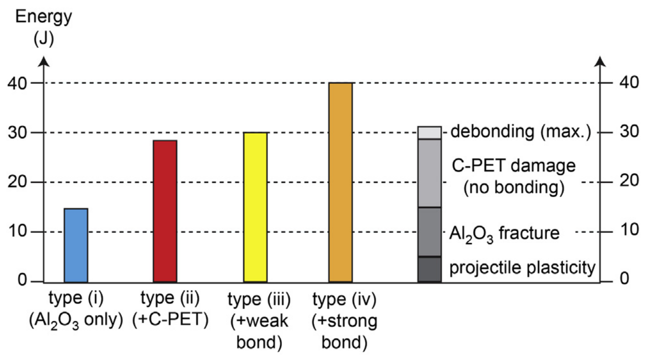

Fig. 12. Schematic representation of the energies associated with penetration by the projectile (with incident kinetic energy of about 50 J) for the 4 different types of sample, and of the approximate contributions from different energy absorption modes.

accounted for solely by that required to effect complete interfacial debonding. It seems likely that this is due to an increased energy contribution from deformation and damage of the composite plate.

Acknowledgements

Financial support for this work was provided by TenCate and EPSRC. The authors are grateful for useful discussions with TenCate personnel, including Dr. Helle Specht and Dr. Paul Bourke. The TenCate grant number was RG 57469. The work also formed part of the EPSRC project with grant number RG 62695.

References

[1] Cantwell WJ, Morton J. The impact resistance of composite materials — a review. Composites 1991;22:347–62.
[2] Woodward RL, Gooch Jr WA, O'Donnell RG, Perciballi WJ, Baxter BJ, Pattie SD. A study of fragmentation in the ballistic impact of ceramics. Int J Impact Eng 1994;15:605–18.
[3] Zaera R, Sanchez-Saez S, Perez-Castellanos JL, Navarro C. Modelling of the adhesive layer in mixed ceramic/metal armours subjected to impact. Compos A — Appl Sci Manuf 2000;31:823–33.
[4] Yadav S. Penetration resistance of laminated ceramic/polymer structures. Int J Impact Eng 2003;28:557–74.
[5] Bendor G, Dubinsky A, Elperin T. Optimization of two-component composite armor against ballistic impact. Compos Struct 2005;69:89–94.
[6] Tasdemirci A, Hall I. Numerical and experimental studies of damage generation in multi-layer composite materials at high strain rates. Int J Impact Eng 2005;34:189–204.
[7] Sarva S, Nemat-Nasser S, McGee J, Isaacs J. The effect of thin membrane restraint on the ballistic performance of armor grade ceramic tiles. Int J Impact Eng 2007;34:277–302.
[8] Feli S, Asgari MR. Finite element simulation of ceramic/composite armor under ballistic impact. Compos Part B — Eng 2011;42:771–80.
[9] Karthikeyan K, Russell BP, Deshpande VS, Fleck NA. Multi-hit armour characterisation of metal-composite bi-layers. J Mech Mater Struct 2012;7:721–34.
[10] Hetherington JG, Rajagopalan BP. An investigation into the energy absorbed during ballistic perforation of composite armours. Int J Impact Eng 1991;11:33–40.
[11] Chocron Benloulo IS, Sanchez-Galvez V. A new analytical model to simulate impact onto ceramic/composite armors. Int J Impact Eng 1998;21:461–71.
[12] Hazell PJ, Appleby-Thomas G. A study on the energy dissipation of several different CFRP-based targets completely penetrated by a high velocity projectile. Compos Struct 2009;91:103–9.
[13] Chen HC, Chen YL, Shen BC. Ballistic resistance analysis of double-layered composite material structures. Theor Appl Fract Mech 2012;62:15–25.
[14] Moriniere FD, Alderliesten RC, Benedictus R. Low-velocity impact energy partition in GLARE. Mech Mater 2013;66:59–68.
[15] Naik NK, Kumar S, Ratnaveer D, Joshi M, Akella K. An energy-based model for ballistic impact analysis of ceramic-composite armors. Int J Damage Mech 2013;22:145–87.
[16] Grujicic M, Pandurangan B, d'Entremont B. The role of adhesive in the ballistic/structural performance of ceramic/polymer-matrix composite hybrid armor 2012;41:380–93.
[17] Tasdemirci A, Tunusoglu G, Guden M. The effect of the interlayer on the ballistic performance of ceramic/composite armors: experimental and numerical study. Int J Impact Eng 2012;44:1–9.
[18] Charalambides PG, Cao HC, Lund J, Evans AG. Development of a test for measuring the mixed mode fracture resistance of bimaterial interfaces. Mech Mater 1990;8:269–83.
[19] Howard SJ, Phillipps AJ, Clyne TW. The interpretation of data from four-point bend testing to measure interfacial fracture toughness. Composites 1993;24:103–12.
[20] Davidge RW, Phillips DC. The significance of impact data for brittle nonmetallic materials. J Mater Sci 1972;7:1308–14.
[21] Johnson GR, Cook WH. Fracture characteristics of three metals subjected to various strains, strain rates, temperatures and pressures. Eng Fract Mech 1985;21:31–48.
[22] Johnson GR, Holmquist TJ. An improved computational constitutive model for brittle materials. In: Schmidt SC, Shaner JW, Samara GA, Ross M, editors. AIP Conference Proceedings, vol. 309; 1994. p. 981–4.
[23] Oberg E. Energy-based mechanics of ballistic impact on ceramic/composite protective plates [PhD thesis]. UK: University of Cambridge; 2013. p. 75–100.